Smart Materials and Structures, 2010, Volume 19, Number 6, 065011

Accurate measurement of piezoelectric coefficient of thin films by eliminating substrate bending effect using spatial scanning laser vibrometry

Glenn J T Leighton and Zhaorong Huang

Department of Materials, Cranfield University, Bedfordshire, MK43 0AL, United Kingdom.

E-mail: g.j.t.leighton@cranfield.ac.uk, z.huang@cranfield.ac.uk

ABSTRACT

One of the major difficulties in measuring the piezoelectric coefficient $d_{33,f}$ for thin films is the elimination of the contribution from substrate bending. We show by theoretical analysis and experimental measurements that by bonding thin film piezoelectric samples to a substantial holder the substrate bending can be minimized to a negligible level. Once the substrate bending can be effectively eliminated, single beam laser scanning vibrometry can be used to measure the precise strain distribution of a piezoelectric thin film under converse actuation. A significant strain increase toward the inside edge of the top electrode (assuming a fully covered bottom electrode) and a corresponding strain peak in the opposite direction just outside the electrode edge were observed. These peaks were found to increase with the increasing Poisson's ratio and transversal piezoelectric coefficient of the piezoelectric thin film. This is due to the non-continuity of the electric field at the edge of the top electrode, which leads to the concentration of shear stress and electric field in the vicinity of the electrode edge. The measured $d_{33,f}$ was found to depend not only on the material properties such as the electromechanical coefficients of the piezoelectric thin films or elastic coefficients of the thin film and the substrate, but also on the geometry factors such as the thickness of the piezoelectric films, the dimensions of the electrode, and also the thickness of the substrate.

I. INTRODUCTION

Piezoelectric films especially lead zirconate titanate (PZT) have attracted considerable attention[1] recently because they can provide functionality for micro-electromechanical systems (MEMS) devices such as micromotors[2], micropumps[3], and chemical sensors[4]. Accurate knowledge of the piezoelectric coefficients d_{ij} of the films is essential for the effective devices modelling and design and process qualification, but their accurate measurement is by no means straightforward. Large discrepancies exist among the reported film piezoelectric coefficients in the literature and these cannot be explained simply by inconsistence of film quality and varies measurement techniques.[5] It is well known that the longitudinal piezoelectric coefficient (d_{33}) of thin films differ from that of bulk materials, hence it is denoted as $d_{33,f}$. If no lateral strain is possible due to the substrate clamping, then:

$$d^{c}_{33,f} = d_{33} - 2d_{31} \frac{s^{E}_{13}}{(s^{E}_{11} + s^{E}_{12})} \qquad (1)$$

Where the s_{ij} are the unclamped mechanical compliances of the piezoelectric film, d_{31} is the unclamped transverse piezoelectric coefficient and $d^{c}_{33,f}$ is called the constrained piezoelectric coefficient [6].

Extensive efforts have been made to measure the $d_{33,f}$ in the past. One of the main difficulties associated with measuring $d_{33,f}$, is how to overcome substrate bending caused by the transverse strain of the actuated piezoelectric film. The 'Berlincourt meter' measuring the direct piezoelectric effect is usually used for bulk ceramics and is not suited to measuring thin films. It is very difficult to produce a homogeneous uni-axial stress on a thin film deposited on thick substrate, without also generating a bending effect, which produces a large amount of charge through the transverse piezoelectric effect [7]. To reduce the substrate interactions

modifications such as pneumatic pressure rig [8] and sample flexure [9, 10] techniques have been developed. The use of piezo-response force microscopy (PFM) measurements for those films with deposited top electrodes may also suffer from the substrate bending effect As for PFM for films without a top electrode; it detects the local vibrations induced by a testing sinusoidal signal, applied between the conductive tip of the atomic force microscopes cantilever and the bottom electrode of the film. Since the radius of the tip apex is in the range of tens of nanometres, the measured piezoelectric response is grain dependent. For some grains, the contribution from d_{15} may be significant, and the measured out-of-plane piezoelectric response could be substantially different from the effective value along the poling direction.[11]

Single beam laser interferometry techniques have difficulty in separating the bending of the substrate from the thickness dilatation of films. Double-beam interferometers have been suggested as a technique to compensate for the bending of the substrate.[12, 13] Dual beam interferometry is believed by many to be a reliable technique to measure the $d_{33,f}$ despite it not being the most user friendly technique, as it requires a stable environment and has a relatively large spot size. Some additional problems are the requirement of high reflectivity for both the front and back surfaces which makes it difficult if not impossible for the measurement of porous thick films. Moreover, if the front and back side beams are not aligned precisely, to be coincident, then substrate bending can contribute substantially to the measured displacement (this will be discussed further in section 2).

Laser scanning vibrometry (LSV) is becoming more popular for $d_{33,f}$ measurements,[14] due partly to the ease of use and the capability of phase related surface scanning measurements. LSV can work in a normal laboratory environment and does not require the sample surface to have a very high reflectivity. LSV measures vibration velocity, which when integrated gives the displacement of the sample.

Recent works on the finite element modelling of the piezo-response of piezoelectric thin films, suggest that the vertical displacement of the top surface of the film when activated by an electric voltage, is the congruence of a number of contributions, such as: the intrinsic piezo-strain, the strain induced by the substrate constraints, the local deformation of the substrate and the top and bottom electrodes, and substrate bending. It is well recognized that the substrate bending displacement could be several times that of the intrinsic piezo-strain, therefore it has to be eliminated completely or compensated for in the measurement.[12, 13] The substrate constraint induced strain is dependent upon the exact boundary conditions, and diminishes if the top electrode dimension is much smaller than the film thickness.[15, 16] The effect of the top electrode is negligible if the film is fully or free from constraint with the substrate.[16] The local deformation of the bottom electrode and substrate is much more complex and could account for more than 70% of the measured displacement.[15] Further detailed modelling has revealed that the local deformation depends on the dimension of the top electrode, film thickness and also the ratio between the two.[5, 17] Only when the dimension of the top electrode exceeds a certain size (a few mm) can the measured piezoelectric coefficient $d_{33,f}$ converge to the constrained $d_{33,f}^{c}$.[17]

The requirement for the top electrode to be larger than a few mm has serious implications since many MEMS devices are less than one mm in all critical dimensions. Also the chance of an electrical short in some thin films, such as those prepared by sol-gel, significantly increases when top electrodes are larger than 1 mm due to the existence of pin-holes. The conclusions from the numerical modelling posses a series questions such as: Can this be confirmed by experiments? Are there other factors which also affect the measured piezo-coefficient?

In this manuscript we report the analysis, modelling and LSV measurement of piezoelectric thin film behaviour under activation with an electric field. We show that the effect of

substrate bending can be eliminated by bonding the back of thin film samples to a large mass. The dependence of the measured piezoelectric coefficients on the size of the top electrode is demonstrated and compared to numerical modelling results. Factors affecting the line profile of piezo-response across the diameter of the top electrode are also discussed.

II. THEORETICAL ANALYSIS

A. Substrate bending without bonding

When an electric field E_3 is applied to a piezoelectric film deposited on a substrate, it bends due to the transversal piezoelectric effect d_{31} (Figure 1(a)). By making the assumption that the specimen is a strip, it can be treated as a unimorph beam simplifying the analysis.[18, 19] Assuming the specimen is simply supported, the curvature κ of the bending can be calculated by:

$$\kappa = \frac{6AB(1+B)}{A^2B^4 + 2A(2B + 3B^2 + 2B^3) + 1} \cdot d_{31} \frac{E_3}{t_p} \tag{2}$$

The bending displacement δ at L_1 (Figure 1(a)) is:

$$\delta = \frac{1}{2}\kappa L_1^{\ 2} = \frac{L_1^{\ 2}}{2t_p} \cdot \frac{6AB(1+B)}{A^2B^4 + 2A(2B + 3B^2 + 2B^3) + 1} \cdot d_{31}E_3 \tag{3}$$

And the slope α at the L_1 is:

$$\alpha = \kappa L_1 = \frac{L_1}{t_p} \cdot \frac{6AB(1+B)}{A^2B^4 + 2A(2B + 3B^2 + 2B^3) + 1} \cdot d_{31}E_3 \tag{4}$$

The displacement between L_2 and L_1 is α (L_2-L_1) (Figure 1(a)) and the total displacement at L_2 is:

$$\Delta = \delta + \alpha\ (L_2 - L_1) \qquad (5)$$

Where $A = Y_m / Y_p$, $B = t_m / t_p$, Y_m is the Young's modulus of the substrate layer, Y_p is the Young's modulus of piezoelectric layer, t_m the thickness of the substrate layer and t_p the thickness of the piezoelectric layer.

For a typical specimen, comprising PZT as the piezoelectric material and silicon (Si) as the substrate with typical values of: Y_m= 130 Gpa, Y_p= 80 Gpa, t_m = 0.25 mm, t_p = 0.001 mm, L_1= 1 mm, L_2 = 10 mm, E_3= 1 MV, and d_{31}=100 pm/V. This gives κ~6x10^{-3} m^{-1}, δ~3 nm, $\alpha(L_2$-$L_1)$ ~53 nm, and Δ ~56 nm! For a d_{31}=100 pm/V assuming the $d_{33,f}$ ~100 pm/V or smaller therefore the thickness dilatation is 100 pm, meaning the contribution from the bending displacement is much larger than the longitudinal piezoelectric displacement. This analysis agrees with the conclusions obtained in literature where it was assumed that the top electrode covers the whole top surface of the PZT.[13]

If the front and back beams are perfectly aligned during double beam interferometry, substrate bending should not contribute anything to the measured displacement. However, if there is a misalignment of l_s, the measured displacement also includes a contribution from the bending effect. This can be estimated from (3). Assuming the front beam is at the centre and the back side beam is misaligned by l_s= 0.2 mm, using the parameters the same as in the previous paragraph and notice B>>1, then the bending contribution δ_s $\sim \frac{l_s^{\,2}}{2t_p} \cdot \frac{6}{AB^2 + 4B} \cdot d_{31} E_3 \sim \frac{l_s^{\,2}}{t_m} \cdot \frac{3}{AB + 4} \cdot d_{31} E_3$~120pm, which is more than the thickness dilatation! So the precise alignment of the back and front beams is of critical importance to

the accurate measurement of the piezoelectric coefficient for thin films using the double-beam interferometer technique.

B. Substrate bending of glue bonding device to a sample holder

The above estimation has assumed that the specimen was simply supported on the sample holder. If however the back of the substrate is bonded to a rigid sample holder, we can show that the bending of the substrate is dramatically reduced, and can be considered to be negligible.

When a positive voltage is applied to the sample, an upward bending moment M_{eq} is induced and the specimen moves upward until it is counter-balanced by the stretched bonding layer (for example, acrylate glue). The bonding layer can be considered as a spring with the spring constant $k = cA/h_{ep}$, where A is the contact area of the acrylate glue with the substrate.[20, 21] For simplicity assuming the maximum displacement of the bottom of the wafer at the edge of the top electrode (L_1) is Z_0 and the displacement is a linear function of the distance from the origin (Figure 1(b)). So the displacement at a position x within the top electrode is xZ_0/L_1.

Considering a small area w_{ep}dx where w_{ep} is the width of the acrylate glue layer and dx is a small length at the position x. Then the force produced by the acrylate glue area w_{ep}dx which acts upon the specimen is $xcw_{ep}Z_0/h_{ep}L_1$dx and the moment is $x^2cw_{ep}Z_0/h_{ep}L_1$. Between L_1 and L_2, the displacement is $(L_2-x)Z_0/(L_2-L_1)$, the force is $(L_2-x)cw_{ep}Z_0/h_{ep}(L_2-L_1)dx$ and the moment is $x(L_2-x)cw_{ep}Z_0/h_{ep}(L_2-L_1)dx$. The total moment by the acrylate glue layer is M and:

$$M = \int_0^{L_1} x^2 \frac{cw_{ep}}{h_{ep}} \frac{Z_0}{L_1} dx + \int_{L_1}^{L_2} x(L_2 - x) \frac{cw_{ep}}{h_{ep}} \frac{Z_0}{L_2 - L_1} dx$$
$$= \frac{1}{6} \frac{cw_{ep}}{h_{ep}} Z_0 (L_2^2 + L_1 L_2) \quad (6)$$

The equivalent bending moment M_{eq} can be obtained by unimorph theory:[18]

$$
\begin{aligned}
M_{eq} &= \frac{wt^2Y_p}{4}\cdot\frac{2AB}{(AB+1)(B+1)}\cdot d_{31}E_3 \\
&= \frac{wY_pt_p^2}{4}\cdot\frac{2AB(1+B)}{(AB+1)}\cdot d_{31}E_3
\end{aligned}
\tag{7}
$$

Where $t = t_m + t_p$. Z_0 can then be obtained by setting $M = M_{eq}$. Then, the ratio of Z_0 and the longitudinal piezoelectric displacement is:

$$
\begin{aligned}
\frac{Z_0}{d_{33,f}E_3t_p} &= \frac{wY_pt_p}{4}\cdot\frac{2AB(1+B)}{(AB+1)}\cdot\frac{6h_{ep}}{cw_{ep}(L_2^2+L_1L_2)}\cdot\frac{d_{31}}{d_{33,f}} \\
&= \frac{Y_p}{4c}\cdot\frac{2AB(1+B)}{(AB+1)}\cdot\frac{6h_{ep}t_p}{(L_2^2+L_1L_2)}\cdot\frac{w}{w_{ep}}\cdot\frac{d_{31}}{d_{33,f}} \\
&\approx 1*10^{-2}\cdot\frac{w}{w_{ep}}\cdot\frac{d_{31}}{d_{33,f}}
\end{aligned}
\tag{8}
$$

Here, we have used the same values as before for the pertinent parameters and a large acrylate glue thickness value h_{ep} = 0.05mm. The minimum acrylate glue width used to bond the sample to the substrate is the width of the top electrode w and usually $w_{ep}>>w$, roughly $d_{31} \sim d_{33,f}$, so the maximum value between the peak back surface displacement Z_0 and the piezoelectric displacement is no more than 1%. If the acrylate glue width is greater than the width of the top electrode which is usually the case, this ratio is even smaller. This indicates that the sample bending effect can be safely ignored if the specimen is glued to a rigid sample holder. Experimental work on low electromechanical coupling thin films reported in the literature supports the above analysis, Muensit and Guy were able to obtained d_{33}= 2.0 pm/V for gallium nitride thin films by gluing the specimen to a thick brass plate, which was in turn rigidly attached to an optical stage.[22] Lueng *et al*. measured d_{33}=2.13 pm/V for gallium

nitride thin films with a heterodyne interferometer.[23] They used silver epoxy to glue the Si substrate to an aluminium block which in turn was rigidly attached to a translation stage.

III. EXPERIMENTAL

A. Device fabrication

A Sol-Gel PZT was synthesized using: lead acetate trihydrate, zirconium propoxide and titanium butoxide precursors. The precursors were stoichiometrically mixed and refluxed in a solution of acetic acid and methanol. The lead excess was fixed at 10 and 20% for final compositions of $Pb_{1.1}(Zr_{0.30}Ti_{0.70})O_3$ and $Pb_{1.2}(Zr_{0.52}Ti_{0.48})O_3$ respectively, the lead excess counteracts lead loss during pyrolysis and subsequent high temperature annealing. The sols were diluted to 0.4M with acetic acid based on lead concentration, which fixes the thickness per layer at approximately 70 nm when spin coated at 3000 rpm.

A 350 μm thick double side polished <100> Si wafer, with a surface oxide (SiO_2) of 200 nm, was platinised using sputtering in a Nordiko RF/DC sputtering machine, 8 nm of RF sputtered titanium was used as an adhesion layer for the 100 nm thick DC sputtered platinum which acts as both bottom electrode and seeding layer for the PZT film. A 1.1 μm thick film of the $Pb_{1.2}(Zr_{0.52}Ti_{0.48})O_3$ and a 2μm thick film of the $Pb_{1.1}(Zr_{0.30}Ti_{0.70})O_3$ were grown upon the platinised Si wafers by; spin coating a PZT layer at 3000 rpm for 30 seconds, followed by pyrolisation at 350°C, then annealing at 560°C for 5 minutes to fully crystallize the layer, this cycle was then repeated 15 times to give a layer of 1.1 μm, the orientation of the PZT films was determined using a θ-2θ X-ray diffraction measurement with a Siemens D5005 diffractometer with a Cu-Kα source. A lift-off lithography process incorporating LOR2A and S1818 resists was used to deposit a patterned top electrode with the thicknesses as the bottom electrode/seed layer. Following the deposition of the top electrode and subsequent lift off, the wafer was RF sputter coated with a blanket layer of gold 200 nm thick, a 2.5 μm thick resist

mask was patterned upon the gold layer using the image reversal resist AZ5214E to provide a mould. 1 μm of nickel was then electroplated into the resist mould which was then stripped giving a hard metal mask for the reactive ion etching (RIE) of the PZT film. The exposed gold and the PZT film was etched using RIE with 120 watts power in Ar and CHF_3 gasses, which gave an etch rate of 1.7 nm/min for a total etch time of approximately 11 hours. After the etching of the PZT, the hard mask was removed by wet etching the nickel in ferric chloride, and removing the gold in potassium iodide and iodine. The wafer was then patterned using AZ4562 resist to RIE etch the bottom electrode and the surface oxide with Ar and CHF_3, O_2 gasses respectively. After this the wafer was patterned on the back face using the same image reversal technique as the front to allow the sputter deposition and subsequent lift off of a 100 nm thick aluminium layer which acts as the hard mask for deep RIE with SF_6 and C_4F_8 through the Si wafer to release the devices. The final step was the O_2 plasma ashing of the protective resist on the front of the wafer and chemical cleaning using acetone and isopropanol alcohol. A Schematic of the side elevation and an image of the device are shown in figure 2.

After processing, the devices were checked to make sure they were viable by measuring their electrical properties (loss and phase) using a Wayne Kerr 6425 precision component analyser. The passed devices were then contact poled using 130°C for 5 minutes with an electric field of 15 MV/m.

B. Device mounting

The glues for bonding the devices to a substantial substrate were chosen to be UV cured, the reason for this is that UV curable glue has a long working time in a yellow light clean room. The chosen glues were from DELO industrial adhesives, DELO-PHOTOBOND 4468 and GB310 which have a young’s modulus of 250 and 1600 MPa respectively. A 100 mm diameter glass plate was coated with glue by spin coating at 2000 rpm, the devices were

placed on the plate which was then loaded into a Karl Suss MA56 mask aligner which UV cured the adhesive using hard contact mode to give the thinnest possible layer of glue (approximately 2 μm for GB310).

C. $d_{33,f}$ Measurement

The Polytec vibrometer system (MSV300) is a modified Mach-Zehnder type interferometer based on the Doppler frequency shift. The $d_{33,f}$ was measured using the MSV300 laser vibrometer of the Polytec MMA 300, using a single HeNe laser beam focussed through a 1.25x objective giving a field of view approximately 7 mm^2. Because the samples were thin film materials, their optical reflectance was excellent and the return signal observed on the vibrometer from the surface was close to 100%. This gave a very good signal to noise ratio, with the noise floor being < 1pm at 9 kHz (figure 3).

The actuating signal was set at 1.8 V_{p-p} to avoid second harmonic generation of non linear effects in the piezoelectric material, which have a destabilising effect on the $d_{33,f}$ measured at the actuated frequency as is shown in figure 4. A sample was actuated with 1 to 8 volts applied signal (2.4 - 22.6 V_{p-p}), investigation of the data shows only the measurements from 1-3 V have a linear increase in the displacement. The measurements were performed within a frequency window of 20 kHz allowing the appearance of a second harmonic at twice the fundamental frequency with 3 V applied signal (figure 3). Each measurement point in the grid for a scan or any single point measurement was averaged over 20 cycles, using complex averaging.

IV. RESULTS AND DISCUSSIONS

A piezoelectric thin film sample with a 500 μm top electrode was measured prior to being constrained by glue bonding to a substrate (figure 5 (un-bonded)). It is evident from figure 5 that there is over ten times displacement contribution from substrate bending, when the

displacement is compared to that of the same sample after it has been bonded to a substrate (figure 5 (bonded)). The unsymmetrical appearance of the trace in figure 5 (un-bonded) is due to point clamping of the sample by the contacting probes, the positions of the two probes have been delineated by the dots upon the trace. The two vertical lines show the position of the top electrode, and it is clear from the trace that there is a linear nature to the substrate bending outside the top electrode.

Figure 5 (bonded) shows the LSV measured surface displacement profile across the top electrode for the same sample after its back was bonded to the sample holder. As for figure 5 (bonded), it is evident from the profile that the substrate away from the actuated (top electrode) area of the piezoelectric is flat having near zero bending, with ripples within the noise floor of the vibrometer < 1 pm. This confirms our analytical conclusion, that, by bonding a thin film specimen to a large mass substrate bending would be reduced. However, the displacement profile across the top electrode is not flat, as can be seen from both figure 4 and 5, there is a significant strain increase toward the inside edge of the top electrode and a corresponding strain peak in the opposite direction just outside the electrode edge.

The positioning dependence in the displacement across the top electrode gives rise to confusion as to what should be defined as the $d_{33,f}$. We defined $d_{33,f}$ as equal to the displacement at the centre (A) (all captions for position reference shown in figure 4) of the electroded area with respect to the stationary substrate (D) outside the electroded region.[24, 25] But it could also be defined as the difference between positions A to C as suggested in, or even B to C.[14] We have used, described below, finite element modelling (FEM) ANSYS to reveal the mechanisms by which the piezoelectric stack is deformed at the edges of the electrode upon actuation. A parametric analysis was performed to investigate the influence of d_{31}, d_{15} and Poisson's ratio ν in the generation of the shape of the actuated structure. The material properties for Ferroperm's PZ23 which were used for the PZT; and the Si properties,

are shown in table 1. The formulae[26] used to vary the Poisson's ratio for a strain in the 3 direction is $v = \frac{-S_{12}}{S_{11}}$, the 2D compliance ($S_{ij}$) matrix, was input directly into ANSYS to model the behaviour of the unique shapes at the edge of the PZT layer. Particular attention was paid to the increased longitudinal displacement at the inside edge (B) of the electrode producing a peak, and an anti-phase peak seen at the outside edge (C) of the electrode in figure 4. Numerical calculation has shown that there is a significant concentration of shear stress and electric field at the edge of the top electrode which leads to the displacement peaking at B[25, 27-29], but little has been discussed about its anti-phase peak at C.

The modelling has shown that there is no significant contribution from d_{15} (with electrode diameters >10 μm) to the appearance of the peaks at the edge of the electrode, but that both the Poisson's ratio v and d_{31} do contribute to the effect. Figure 6 shows the modelling results for PZT with different Poisson's ratios whilst all other parameters were kept constant. It is evident that the Poisson's ratio of the piezoelectric material has a large impact on the generation of the two peaks at the edge of the electrode. The original Poisson's ratio of the material used for the modelling is 0.34, as this increases the $d_{33,f}$ decreases and the peaks become more pronounced as shown by the trace with a Poisson's ratio of 0.435. If it is reduced to 0.01, as can be seen in figure 6, then the $d_{33,f}$ value of -297 pm/V is very close to the d_{33} (-327 pm/V) of the material used in the model. Notice the peak and the anti-phase peak at two sides of the edge of the top electrode appear in pairs: when there is no peak at the position B, no anti-phase peak exists at the position C.

The same parametric modelling was performed varying d_{31} whilst all other parameter were kept constant, the results which are shown in figure 7 show a similar trend as that of figure 6 where Poisson's ratio was varied, but in figure 7 the $d_{33,f}$ more closely resembles the materials d_{33} as is suggested by (1). Again the peak at B and the anti-phase peak at C at the edges of the

top electrode appear in pairs, suggesting they are both related to the concentration of electric field and shear stress at the vicinity of the edge of the electrode. Therefore they should not be considered in the definition of $d_{33,f}$. From these considerations, $d_{33,,f}$ is best to be defined as the displacement at the centre A of the electrode relative to the stationary substrate D outside the electroded region. According to this definition the $d_{33,f}$ is 30 pm/V in Figure 5.

The displacement profiles across top electrode were found to depend on the size of the top electrode. Samples with 11 different sizes of top electrode, range from 0.3 to 2.0 mm in diameter, were fabricated and poled under exactly the same conditions. Figure 8 shows three representing displacement profiles with different top electrode diameters. When the diameters were 0.3, 0.4, 0.5 and 0.6 mm the displacement profile across the top electrode was almost flat. When the top electrode size was increased further, displacement peaks at the edge of the electrode started to appear, and there is congruence as the height of the peaks increases with the increased diameter of the top electrode.

The measured $d_{33,f}$ as a function of the diameter of the top electrode is shown in figure 9. When the electrode was small (0.3 mm), the specimen showed the highest $d_{33,f}$, and it decreased with the increasing size of the electrode until the electrode diameter reached 1.1 mm in this study. After that, further increase of the electrode size lead to the increased $d_{33,f}$, until it conformed to a value when the electrode diameter is larger than 1.5 mm for our thin film specimens. This feature of non-monotonic dependence on the electrode size agrees with previous FEM results[5, 17] qualitatively, but further effort on FEM modelling using different elastic and electromechanical material parameters and actual sample dimensions failed to produce a profile matching exactly the measurement results shown in figure 9. Although the maximum and minimum displacements were matched, the FEM minima of the displacement always appeared at around the 0.1 mm electrode diameter, rather than the experimental value of 1.1 mm. Reasons for this discrepancy are not clear. A possible explanation is related to

the poling of the thin films. Numerical calculations have shown concentrations of electrical field and shear stress at the edge of top electrode and the existence of electric fields immediately outside the top electrode area with directions from angles to almost perpendicular to the z-direction.[27, 29] FEM considers the piezoelectric to be perfectly poled in the z-direction due to the way the material properties are entered into the model. When a model is solved we can see the edge displacement features due to the interaction of the electric field with the d_{31} and the Poisson's ratio. What is not considered is that the experimental device is poled with the same radiating electric field, which would give rise to a d_{33} effect along the horizontal direction outside the top electrode area. This could create both an increase in the effective dimensions of the top electrode (which is non trivial in a system measured in microns) and strain relationships outside the top electrode opposite those inside the top electrode. This effect would be more pronounced in small electrode than in larger ones which leads to flat displacement profiles in small top electrodes as described before.

FEM also shows that the size of the electrode when the $d_{33,f}$ reaches its lowest value and at what size it reaches the constrained piezoelectric coefficient $d_{33,f}^{c}$, depends on not only the properties of the piezoelectric materials, but also on the parameters of the substrate such as its thickness and elastic coefficients. This is an addition to the work reported by Wang *et al* [5] where the substrate thickness was fixed. Figure 10 shows the FEM calculated $d_{33,f}$ as functions of electrode radius for different thickness of the Si substrate. The material parameters used for the model conform to those of Wang *et al* [5], and as can be seen from the 500 μm trace in figure 10, our model has the same response as the 5 μm trace (figure 4(a) from ref. 5). Thicker Si substrates led to larger substrate deformation, therefore generally smaller $d_{33,f}$ values, and requires larger electrode sizes to reach the constrained piezoelectric coefficients $d_{33,f}^{c}$. These results indicate that there should be some caution in determining the piezoelectric coefficient d_{33} from the measurement of its thin film on substrate property $d_{33,f}$, since the measured value depends on not only the intrinsic material properties such as the

elastic and electric coefficients of the piezoelectric materials and the substrate, but also on geometrical parameters such as the dimensions of the electrode and also the substrate.

V. CONCLUSIONS

We have presented a theoretical analysis, to show that bonding of thin film piezoelectric samples to a substantial holder can help in $d_{33,f}$ measurements by subjugating substrate bending. This theoretical result has been validated with experimental measurements comparing thin film piezoelectric devices actuated before and after glue bonding. Where the before results showing substrate bending had a displacement peak an order of magnitude greater than the thickness dilatation. After bonding, the specimen showed little substrate bending, and a clamped displacement was found not higher than the noise floor of the measurement system (approximately 1pm).

By using vibrometry for the $d_{33,,f}$ measurements it was possible to do detailed scans of the actuated thin film samples, this highlighted a displacement profile whereby the edges of the electrode had anti-phase peaks. Due to the non-continuity of electric field at the edge of the top electrode, there is a significant concentration of shear stress and electric field in the vicinity of the electrode edge, which lead to a marked increase of strain toward the edge of the top electrode. In association with this strain peaking at the inside edge, there is a strain in opposite direction just outside the electrode. Both FEM modelling and LSV measurements confirmed these results. FEM results also revealed that Poisson's ratio and the d_{31} of the piezoelectric thin film affect the heights of these peaks. Higher Poisson's ratio and larger d_{31} leads to larger strain increase at the electrode edge.

The measured $d_{33,f}$ was found to depend on the size of the top electrode and it is not a monotonic relationship. At very small top electrode sizes (< 1μm), $d_{33,f}$ is close to d_{33}, but decreases with the increasing size of the top electrode, $d_{33,,f}$ then reaches a minimum, before

beginning to increase again with the increasing size of the top electrode, until it reaches the constrained piezoelectric coefficient $d_{33,f}^{c}$, when the top electrode is beyond a certain size. However, this relationship depends not only on the material properties such as the electromechanical coefficients of the piezoelectric thin film and the elastic coefficients of the thin film and the substrate, but also upon the geometrical factors such as the thickness of the piezoelectric film, the dimensions of the electrode, and also the thickness of the substrate.

ACKNOWLEDGEMENTS: The authors acknowledge the financial support of UK EPSRC (EP/D506638/1) and European network of excellence project MIND (NOE 515757-2). The authors would also like to thank Dr. Q Zhang for manufacturing the PZT sols used in these experiments.

References

[1] P. Muralt, J. Am. Ceram. Soc. **91**, 1385 (2008).

[2].K.R. Udayakumar, S.F. Bart, A.M. Flynn, J. Chen, L.S. Tavrow, L.E. Cross, R.A. Brooks, D.J. Ehrlich, *IEEE-MEMS*, Nara, Japan (1991) 109-113.

[3]P. Lugienbuhl, S.D. Collins, G.A. Racine, M.A. Gretillat, N.F.d. Rooij, K.G. Brooks, N. Setter, Sensors and Actuators **A64,** 41 (1997).

[4]J. Xia, S. Burns, M. Porter, T. Xue, G. Liu, R. Wyse, C. Thielen, IEEE International Frequency Symposium, San Francisco, USA (1995) 879.

[5] Z. Wang, G.K. Lau, W. Zhu, and C. Chao, IEEE Trans. Ultra. Ferro. Freq. Contr. **53**, 15-22 (2006).

[6] K. Lefki and G. Dormans, J. Appl. Phys. **76**, 1764 (1994).

[7] A. Barzeger, D. Damjanovic, N. Ledermann and P. Muralt, J. Appl. Phys. 93, 4756 (2003).

[8] F. Xu, F. Chu, S. Trolier-McKinstry, *J. Appl. Phys.,* **86,** 588 (1999).

[9] M. Dubois and P. Muralt*, Sensors and Actuators,* **77,** 106 (1999).

[10] J. Southin, S.A. Wilson, D.A. Schmitt and R. W. Whatmore *J. Phys. D:Appl. Phys.* **34**, 1456 (2001).

[11] C. Harnagea C, A. Pignolet A, M. Alexe M and D. Hesse, Integrated Ferroelectrics **44**, 113 (2002).

[12] W.Y. Pan and L.E. Cross, Rev. Sci. Instrum, 60 (1989) 2701-2705.

[13] A. L. Kholkin, Ch. Wutchrich, D.V. Taylor and N. Setter, Rev. Sci. Instrum. 67 (1996) 1935-1941.

[14] K. Yao, F. E. H. Tay, IEEE TUFFC, **50**, 113-116(2003).

[15]J.H. Li, L.Chen, V. Nagarajan, R. Ramesh, and A.L. Roytburd, Appl. Phys. Lett. **84**, 2626-28 (2004).

[16]H. Sato and J. Akedo, J. Am. Ceram. Soc. **89**, 3715-3720 (2006).

[17] Z. Wang and J. Miao, J. Phys. D: Appl. Phys. 41, 035306 (2008).

[18] Q.M. Wang and L. E. Cross, Ferroelectric*s* **215**, 187 (1998).

[19] J. G. Smits and W.S. Choi, IEEE Trans. Ultrason. Ferroelectr. Freq. Control **38**, p. 256 (1991).

[20] Q.M. Zhang, W.Y. Pan and L.E. Cross, J. Appl. Phys. **63**(8), 2492 (1988).

[21] Q.M. Zhang, S.J. Jang and L.E. Cross, J. Appl. Phys. **65**(7), 2807 (1989).

[22] S. Muensit and I.L Guy, Appl. Phys. Lett. **72**, 1896 (1998).

[23] C.M. Lueng, H.L.W. Chan, C. Surya, W.K. Fong, C.L. Choy, P. Chow, and M. Rosamond, J. Non-Cryst. Solids **254**, 123 (1999).

[24] Z. Huang, Q. Zhang, S. Corkovic, R. Dorey, G. Leighton, R. Wright, P. Kirby and R.W. Whatmore, J. Electroceram, **17**, 549 (2006).

[25] Z. Huang, G. Leighton, R. Wright, F. Duval, P. Kirby and R.W. Whatmore, Sensors and Actuators A-Physical, **135**, 660 (2007).

[26] Y. Li and D.Y. Chung, phys. Stat. sol. (a), **46**, 603 (1978).

[27] J. Yang, The Mechanics of Piezoelectric Structures, World Scientific Publishing, Singapore, 2006.

[28] M. Yoshida, F. narita, Y. Shindo, M. Karaiwa and K. Horiguchi, Smart Mater. Struct. **12**, 972-978 (2003).

[29] L.H. He, and R.Q. Ye, Theoretical and Applied Fracture Mechanics, **33**, 101-106 (2000).

Table 1 Material properties used for FEM (FIG 6 & 7)

Parameter	PZ23	Si
Density (kg/m^3)	7700	2330
Poisons ratio		0.23
Young's modulus (GPa)		130
c_{11} (GPa)	157	165
c_{12} (GPa)	109	63.9
c_{13} (GPa)	97.7	
c_{33} (GPa)	123	
c_{44} (GPa)	25.7	79.6
Piezo-properties (C/m^2)		
e_{31}	-1.93	
e_{33}	15.5	
e_{24}	10.81	
Permittivity (C^{2}N^{-1}m^{-2})		
ε_{11}	1370	
ε_{33}	1500	

Figure captions

FIG 1 Schematic of thin film specimen deformation under an applied voltage. (a) simply supported; (b) the back of the substrate is bonded to a rigid sample holder.

FIG 2 Schematic showing the side elevation of the devices used for $d_{33,f}$ measurements, with an image showing a 4mm device with a 800μm top electrode.

FIG 3 Average spectrum FFT showing the appearance of a second harmonic at twice the fundamental with a 3 volt applied signal.

FIG 4 Measured surface displacement across a top electrode with different actuation voltage 1-8 volts highlighting non-linear displacement (e.g. displacement at 1V 10 pm at 8V 55 pm).

FIG 5 Displacement profile for a simply supported sample showing that the substrate bending is larger than the thickness dilatation by the piezoelectric effect (un-bonded trace), when compared to the same sample glued to a sample holder (bonded trace).

FIG 6 FEM displacement profiles showing the effect of varying the Poisson's ratio from 0 to 0.435.

FIG 7 FEM displacement profile for the corresponding sample dimensions as figure 6 but varying the d_{31} from -128E-12 down to -1E-12.

FIG 8 Experimental results showing the impact of the electrode diameter on the $d_{33,f}$ displacement and edge profiles of devices actuated with the same voltage.

FIG 9 A graph of the $d_{33,f}$ displacement of devices from 2mm to 0.3mm electrode diameter showing the size relationship of the top electrode.

FIG 10 FEM modelling showing the effect of the substrate thickness on the $d_{33,f}$ profile.

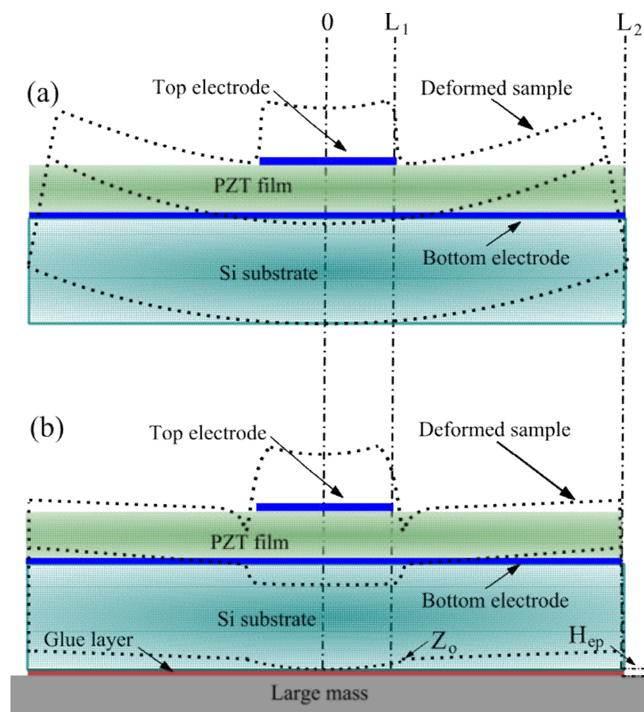

Figure 1

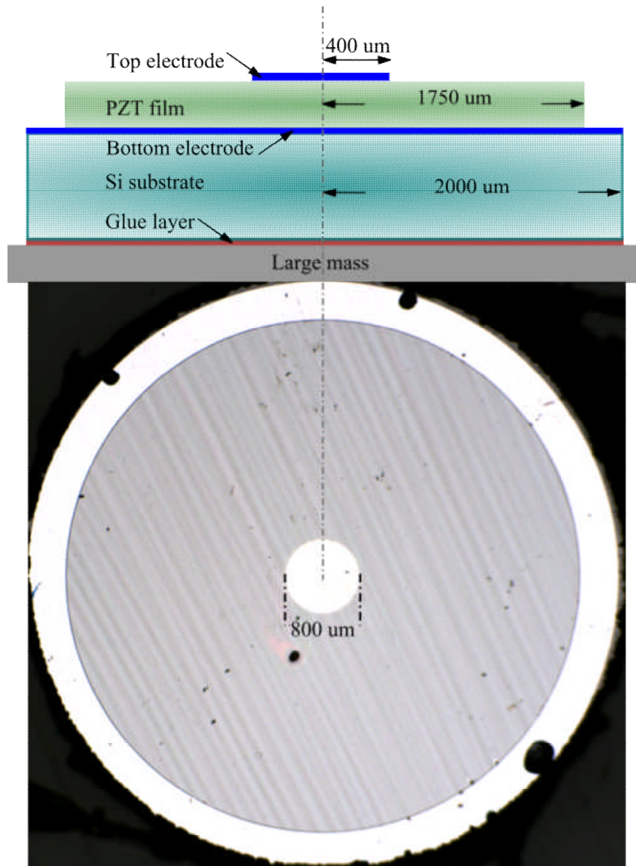

Figure 2

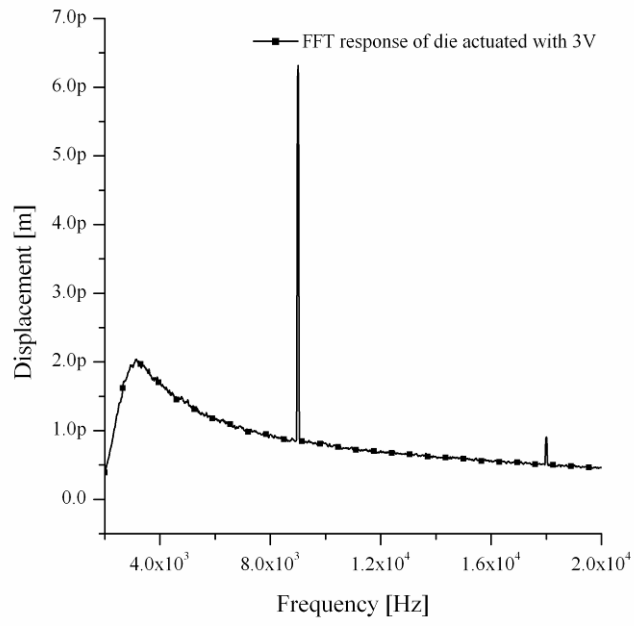

Figure 3

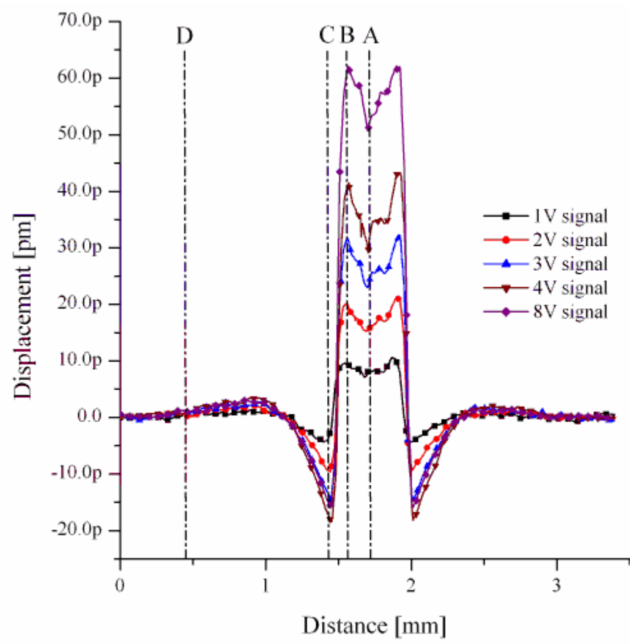

Figure 4

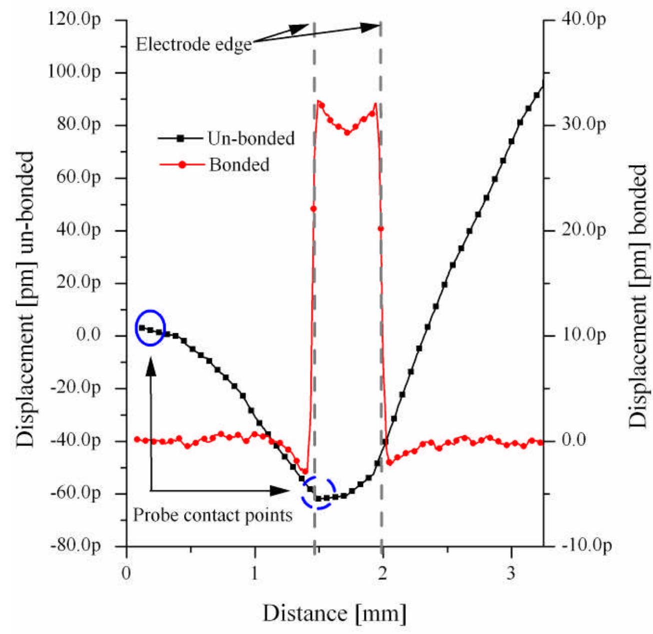

Figure 5

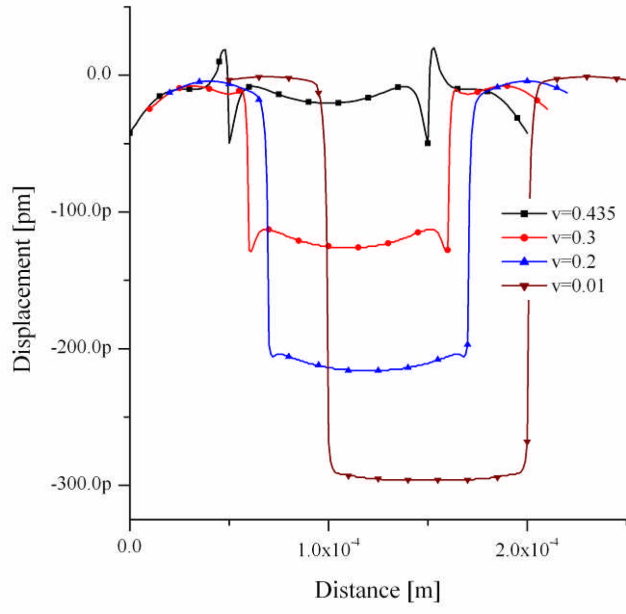

Figure 6

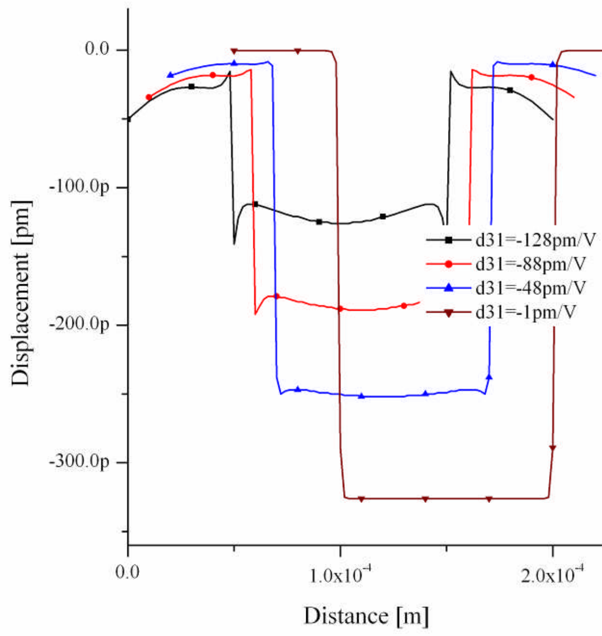

Figure 7

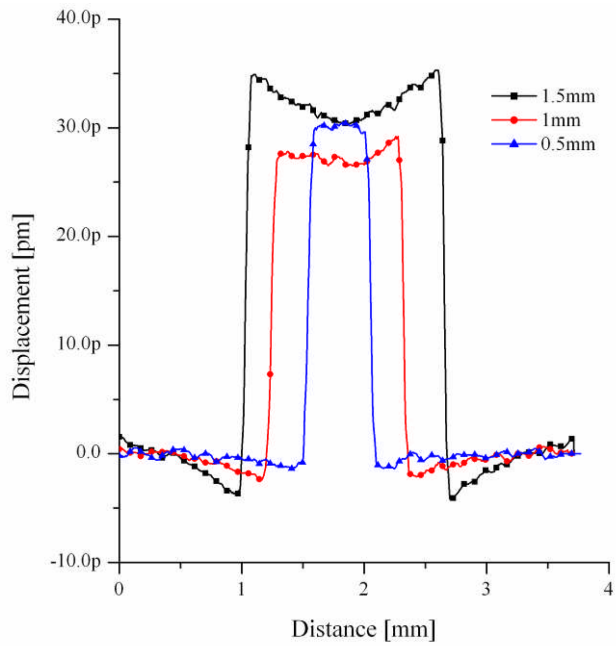

Figure 8

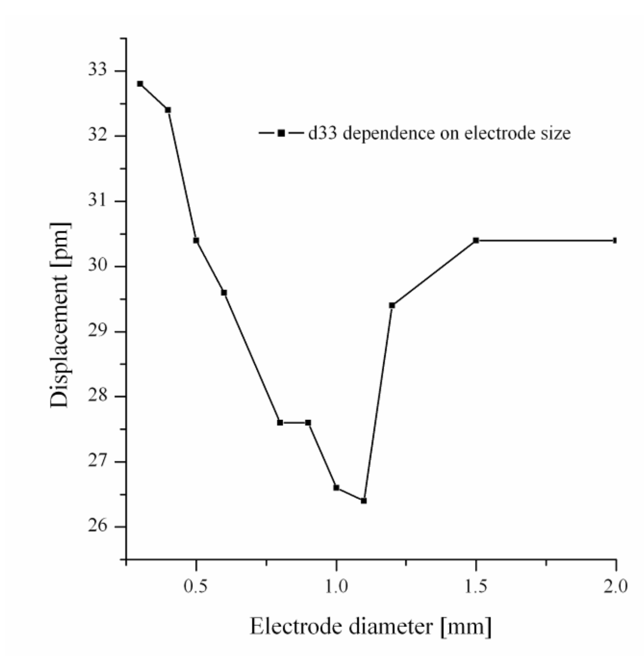

Figure 9

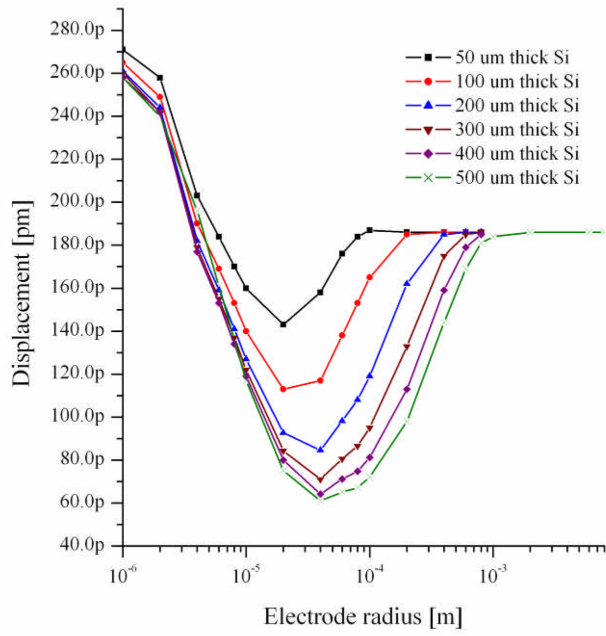

Figure 10